

DNS Investigation for the Taylor-Culick flow Stability Analysis

F. Chedevergne* and G. Casalis† and J. Majdalani‡

ONERA, 2 av. Edouard Belin, BP 4025, 31 055 Toulouse Cedex, FRANCE

Thanks to a global linear stability analysis¹, the intrinsic instabilities responsible of the thrust oscillations arising in large segmented solid rocket motors have been identified. Comparisons between the theoretical predictions coming from the linear stability analysis and experimental results on subscale motors have given excellent agreements². Thus, it appears that the frequency signature of the thrust oscillations characterized by frequency paths is directly due to the merging of the intrinsic instabilities of the flow.

However some points remain unclear in the theoretical approach. In order to analyze these points DNS calculations have been performed. Beyond a simple validation of the theoretical results, these DNS calculations provide a new way to access the interaction that can exist between acoustic modes and intrinsic instabilities inside solide rocket motors.

Nomenclature

ω_i	temporal growth rate
ω_r	circular frequency
θ	azimuthal angle
R	Radius of the model flow
r	radial position
R_0	Radius of the VALDO cold gaz facility
s_{ac}^q	Acoustic part of the physical quantity q : $s_{ac}^q = s_{fluc}^q - s_{th}^q$
s_{fluc}^q	Fluctuating part of the physical quantity q
s_{th}^q	Theoretical evolution of the eigenmode q
t	time
V_{inj}	Velocity injection of the model flow
x	axial position
X_e	length of the truncated domain

Subscripts

$()_i$	imaginary part
$()_r$	real part
-	vector

I. Introduction

LARGE segmented solid rocket motors exhibit thrust oscillations which are due to inflow pressure fluctuations. For years this problem has been investigated, especially in the framework of the P230 development, the booster of the european Ariane 5 launcher. Recently, intrinsic instabilities of the flow have been identified¹ as the primary source of the pressure fluctuations. These instabilities have been found thanks to a linear

*PhD student, Department Models for Aerodynamics and Energetics, Member AIAA.

†Research Engineer, Department Models for Aerodynamics and Energetics, Member AIAA.

‡Jack D. Whitfield Professor of High Speed Flow, Department of Mechanical, Aerospace and Biomedical Engineering, Member AIAA.

stability analysis. Using the results of this approach, successful comparisons² have been done with subscale solid rocket motors measurements³. Moreover cold gas experiments, conducted by G. Avalon⁴ provide a large amount of data in a configuration close to the theoretical model. In this case too, the comparisons between the experimental results and the theoretical ones give a very good agreement. However some points remain unclear and it is necessary to use another approach to validate these results. For that purpose, DNS calculations have been performed.

Before exploring the DNS results, the first part of this paper is dedicated to the linear stability analysis which is used to find out the intrinsic instabilities of the motor flow. The unresolved problems of this stability approach will be pointed out. Then, the computation strategy using DNS calculations will be described. The expected validation of the theoretical results by the DNS results will be investigated. Beyond this validation, it will appear that these calculations highlight interactions between the intrinsic instabilities and acoustic modes.

II. Biglobal Linear Stability Analysis

First we define a model flow standing for the mean flow occurring inside solid rocket motors. The model geometry is a semi-infinite cylinder of radius R . Fluid is injected through the wall at a constant and uniform velocity V_{inj} in the radial direction r , in order to simulate the gas ejection on the combustion surface of the propellant. The lengths and the velocities are made dimensionless with the radius R and the velocity V_{inj} . The semi-infinite cylinder is truncated at $x = X_e$ in order to compute the mean flow thanks to the CEDRE code (ONERA), see the section A of part III. Figs. 2(a) and 3(a) give a view of the mean flow velocity components for $X_e = 8R_0 = 0.24$ m. One notes that this flow is very close to the Taylor-Culick flow^{5,6} except in the front wall region where a boundary layer appears due to the no-slip condition. This flow is computed in the (x, r) plane using the axisymmetric hypothesis and assuming a laminar flow. The agreement obtained between the computed flow and the Taylor-Culick one confirms the incompressible behaviour of the flow. Many measurements, like in the VALDO (radius $R_0 = 0.03$ m) cold gas facility at ONERA Palaiseau, show a very good agreement with the theoretical Taylor-Culick flow. This validates the chosen model flow. The two parameters R and V_{inj} of the model flow are used to made all the physical quantities dimensionless. Thus, a Reynolds number $Re = \frac{\rho R V_{inj}}{\mu}$ is defined and is the only remaining parameter which appears in the Navier-Stokes equations. A stability analysis is performed, based on a perturbation technique such that any physical quantity Q is written as a superposition of a mean value \bar{Q} and a fluctuating part q . The superposition is introduced into the Navier-Stokes equations, and after some simplifications and a linearization, a linear system is obtained which coefficients are functions of the mean flow only.

The perturbation q is searched as :

$$q = \hat{q}(x, r) e^{i(n\theta - \omega t)} \quad (1)$$

because the mean flow depends on x and r and only on them. In this expression, n is an integer and represents the azimuthal wave number, ω is a complex number, its real part stands for the circular frequency and its imaginary part for the temporal growth rate.

As a first study, only the axisymmetric modes are searched, meaning that $n = 0$, and thus a streamfunction ϕ can be defined for the perturbation. The linearized Navier-Stokes equations written for the streamfunction ϕ lead to a partial differential equation (E) in (x, r) of order 4. This equation is solved for $(x, r) \in [0, X_e] \times [0, 1]$. Boundary conditions are imposed for the streamfunction, the critical point is to determine an appropriate outflow condition^{7,8} at $x = X_e$. After discretization in the computational domain, (E) is written as a generalized eigenvalue problem $\underline{\underline{A}} \underline{\underline{\Phi}} = \omega \underline{\underline{B}} \underline{\underline{\Phi}}$. Then, an Arnoldi algorithm⁹ is used to compute the eigenvalues ω and the associated eigenfunctions.

One of the output of the calculation is the set of complex eigenvalues ω which defines the spectrum of the stability problem. An example for $Re = 1975$ is given in Fig. 1. An eigenvector $\underline{\underline{\Phi}}$ is associated to each calculated eigenvalue, which coefficients represent the discretized values of the associated eigenfunction $\hat{\phi}(x, r)$. The whole perturbation $q = \hat{q} e^{-i\omega t}$, *i.e.* $\{u_x, u_r, p\}$, is called mode and can be identified by ω . Once the results of the stability analysis are turned into dimensionnal quantities using the parameters R and V_{inj} , any physical perturbation q for a given mode $\omega = \omega^0$ can be written as :

$$q = A \hat{q} e^{i \frac{V_{inj}}{R} \omega^0 t} = A [(\hat{q})_r \cos(2\pi f t) + (\hat{q})_i \sin(2\pi f t)] e^{\nu t} \quad \text{with } f = \frac{V_{inj}}{2\pi R} \omega_r^0 \quad \text{and } \nu = \frac{V_{inj}}{R} \omega_i^0 \quad (2)$$

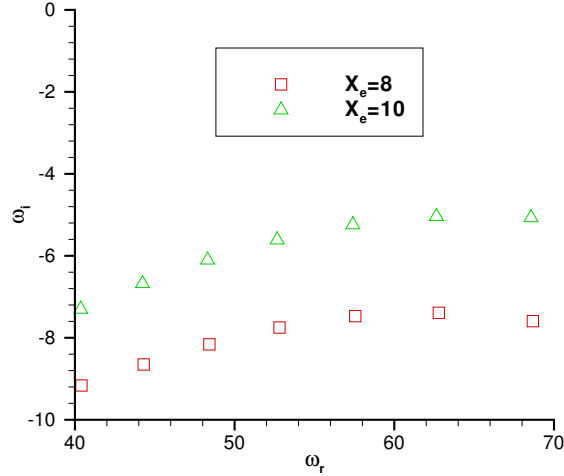


Figure 1. Set of eigenvalues in the complex (ω_r, ω_i) plane for $Re = 1975$. Two cases are shown : $X_e = 8$ (red squares) and $X_e = 10$ (green triangles).

where A is an unknown constant value standing for the initial amplitude of the perturbation. In fact as a solution of a linear system the initial amplitude A of the perturbation q is actually unknown.

Two major results coming from the stability analysis can be pointed out. First the spectrum is discrete. There is only a discrete set of circular frequencies that can develop in the main flow. Second, all the eigenvalues have a negative imaginary part. This means that the modes will be exponentially damped in time. However, the associated eigenfunctions are exponentially growing in the streamwise direction. Figs. 2(b) and 3(b) present the spatial evolution of the real part of the eigenfunctions $\hat{u}_x = \frac{1}{r} \frac{\partial \hat{\phi}}{\partial r}$ and $\hat{u}_r = -\frac{1}{r} \frac{\partial \hat{\phi}}{\partial x}$ associated with the eigenvalue $\omega = 40.409 - 9.164i$ ($X_e = 8R_0$). It clearly shows a strong amplification

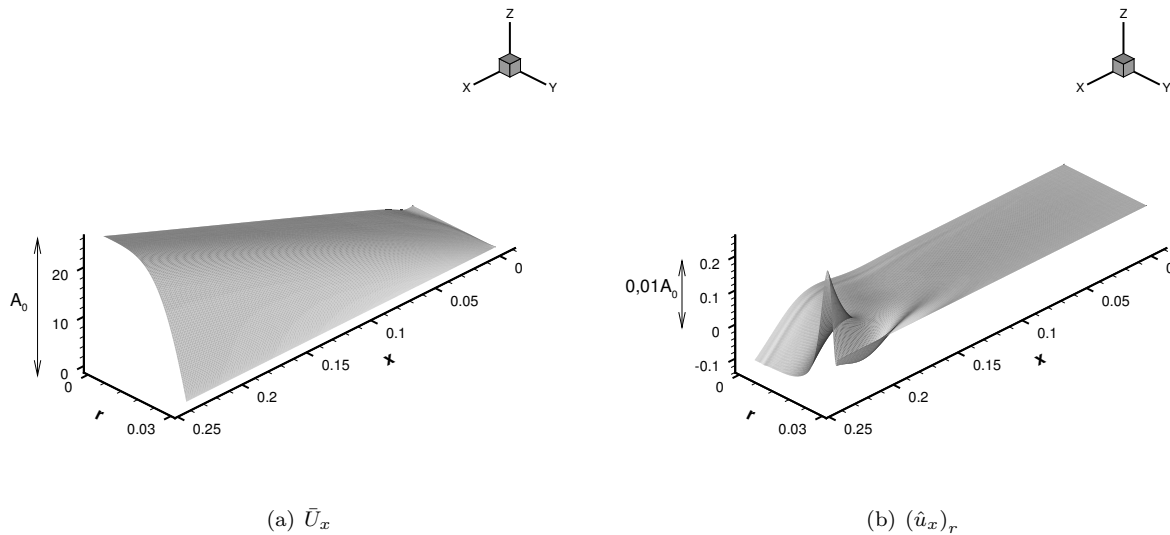


Figure 2. Longitudinal components of the velocities of the basic flow \bar{U}_x and of perturbation \hat{u}_x (real part). Here the initial amplitude A and time of formula 2 are $t = 0$ and $A = 0.01A_0$.

(exponential-like amplification) in the streamwise direction. Thus for a given eigenvalue, there are two opposite effects : the perturbation decreases when time is running and it is exponentially growing in the

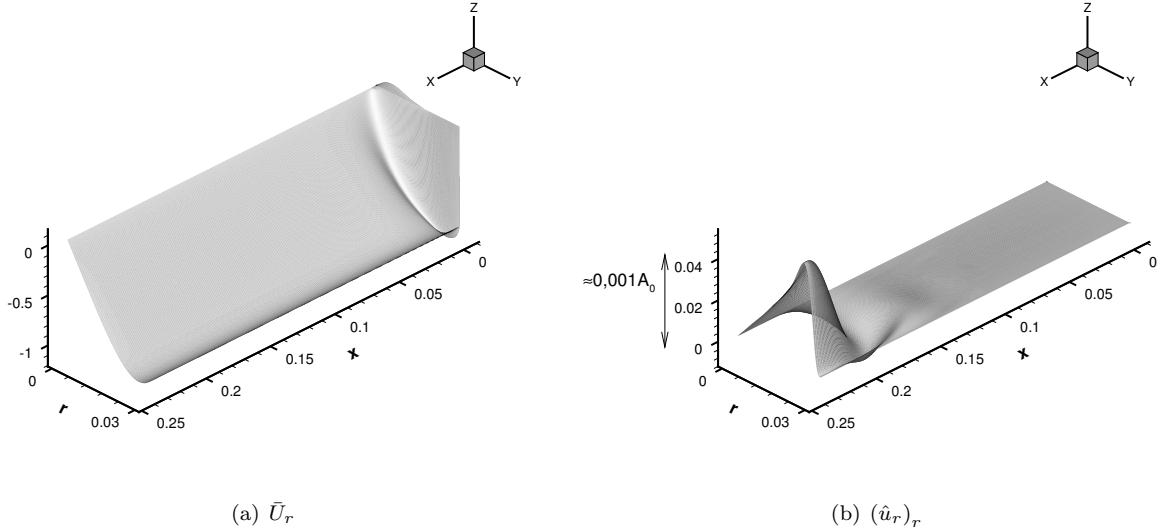


Figure 3. Radial components of the velocities of the basic flow \bar{U}_r and of perturbation \hat{u}_r (real part).

longitudinal direction x .

The stable behaviour of the stability modes has given a new insight on the thrust oscillations arising². The frequency paths observed on all subscale or fullscale solid rocket motors are due to the merging of these intrinsic instabilities of the flow. The merging is believed to result from the coupling between the stability modes and the acoustic ones. The instability modes are excited by some sources (cavity, acoustic modes,...) and are then damped according to the stability theory.

Even if the linear stability analysis has provided the basis of a scenario for the origin of the thrust oscillations, it has also exhibited some unresolved problem. In particular, Fig. 1 illustrate the dependance on X_e of the eigenvalues. There is no physical explanation for such a fact. It is possible that it results from the numerical procedure which could lead to the calling into question of the stability analysis validity. It is thus extremely important to know more about this dependance. DNS calculations are then performed.

III. Direct Numerical Simulation

DNS computations are performed with the use of an ONERA code called CEDRE. The space discretization is based on a finite volume approach and uses an upwind Roe scheme with a second order extension (MUSCL method with Van Leer limiter). A code description can be found in¹⁰ and more specific information concerning the code validation for space applications are given in¹¹.

For the present study, laminar Navier-Stokes computations are performed. In order to be realistic, the characteristic length and velocity are chosen to match the VALDO ones⁴. It means that for the DNS computations the radius of the pipe is $R = R_0 = 0.03$ m and the injection velocity is $V_{inj} = 1$ m/s.

Four meshes have been tested and mesh independency has been checked. The presented results for $X_e = 8R_0$ have been performed with the use of a grid composed of 301×161 nodes (cosine repartition) such that the thickness of the cells on the boundaries is about $3 \mu\text{m}$.

A. Steady calculations

An implicit time scheme is used with a fixed value of the CFL number : $CFL = 10$ for the steady calculations. The purpose of these calculations is to compute the basic flows which are used for the linear stability calculations. It is possible to use the Taylor-Culick flow as basic flow for the stability analysis but it does not satisfy the front wall boundary condition : a no-slip condition at $x = 0$ is indeed mandatory for a viscous flow, which is not satisfied by the Taylor-Culick solution. However, the boundary layer which develops at

$x = 0$ only acts in the vicinity of the front wall, where the fluctuation is nearly zero, see Figs. 2(b) and 2(b), and so the use of the Taylor-Culick solution leads to the same kind of stability results. For more details see¹².

Once the computation is converged, the steady flow is then used as basic flow for the stability calculation.

B. Unsteady calculations

For these computations an explicit time scheme is used with a time step $\Delta t = 5.10^{-9}$ s. The resulting maximum CFL number is lower than 1.

As mentioned above, the goal of the DNS calculations is to validate the results exhibited by the linear stability theory. The adopted strategy is to superimpose at the initial time a stability mode $\omega = \omega_0$, see Figs 2(b) and 2(b) for an example where $\omega_0 = 40.409 - 9.164i$, to the previously computed basic flow, see Figs. 2(a) and 3(a). The initial time t and amplitude A of formula 2 are chosen as $t = 0$ s and $A = 0,01A_0$ where A_0 is the maximum value reached by the longitudinal component \bar{U}_x of the mean flow. It is important to note that the pressure perturbation of the stability mode is not superimposed to the pressure distribution of the mean flow. It does not generate a strong noise at the beginning of the computation because the amplitude of the pressure fluctuation is very low. The process which leads to this superposition is not simple, grid projections must be done without introducing artificial errors. As special attention has been paid on the boundary conditions.

For stability exploration in such a flow, other strategies can be used. For example S. Apte and V. Yang^{13,14} used a white noise or an acoustic excitation to performe LES calculations where instabilities are excited.

Once the superposition is done, the computation is started. The origin of time is defined at this moment : $t = 0$ s. At $t = 0.02$ s, that is to say after 4,000,000 iterations, the calculation is stopped. Signals from different sensors previously defined are analyzed.

C. Three different computed cases

Using the strategy deccribed above, for given values of R and V_{inj} we can performed different computations by changing the eigenmode introduced at $t = 0$ s or the length of the pipe X_e . In this paper, three cases are presented :

- Case 1 corresponds to the introduction of the mode $\omega^0 = 40.409 - 9.164i$ for a pipe length $X_e = 8R_0$.
- Case 2 corresponds to the introduction of the mode $\omega^0 = 40.367 - 7.302i$ for a pipe length $X_e = 10R_0$.
- Case 3 corresponds to the introduction of the mode $\omega^0 = 68.679 - 7.594i$ for a pipe length $X_e = 8R_0$.

The first two cases are actually only differing one from another by the pipe length X_e . On Fig. 1 one can see that the mode $\omega = 40.409 - 9.164i$, calculated for $X_e = 8$, is moving to $\omega = 40.367 - 7.302i$ for $X_e = 10$. It is the same mode.

The acoustic frequencies are functions of the pipe length X_e , see the paragraph 1. For the two first cases, the first acoustic mode has a frequency which is far from the introduced mode frequency $f = \frac{V_{inj}\omega_r^0}{2\pi R_0}$. Af course it is also true for the circular frequencies. Because of this, linear behaviours are expected for the perturbations. Contrary to the two first cases, the third one implies a mode which frequency is very close to the first acoustic mode one. Thus, non linear interactions should act and lead to slightly different results. To illustrate these three cases, Fig. 4 presents a sketch where the circular frequencies are drawn with respect to the pipe length X_e .

IV. Results

A. Case 1

For a truncated domain of length $X_e = 8R_0 = 0.24$ m, the mode $\omega = 40.409 - 9.164i$ is superimposed to the basic steady flow. At $t = 0$ s only the real part of \hat{u}_x and \hat{u}_r , *i.e.* $(\hat{u}_x)_r$ and $(\hat{u}_r)_r$ are added to \bar{U}_x and \bar{U}_r respectively. Let be s_{fluc}^q the difference of the signal of a sensor and its steady part (the value of the corresponding basic flow component). Any signal s_{fluc}^q can be compared to the theoretical evolution s_{th}^q given by formula (2) which rules the temporal behaviour of any fluctuation q according to

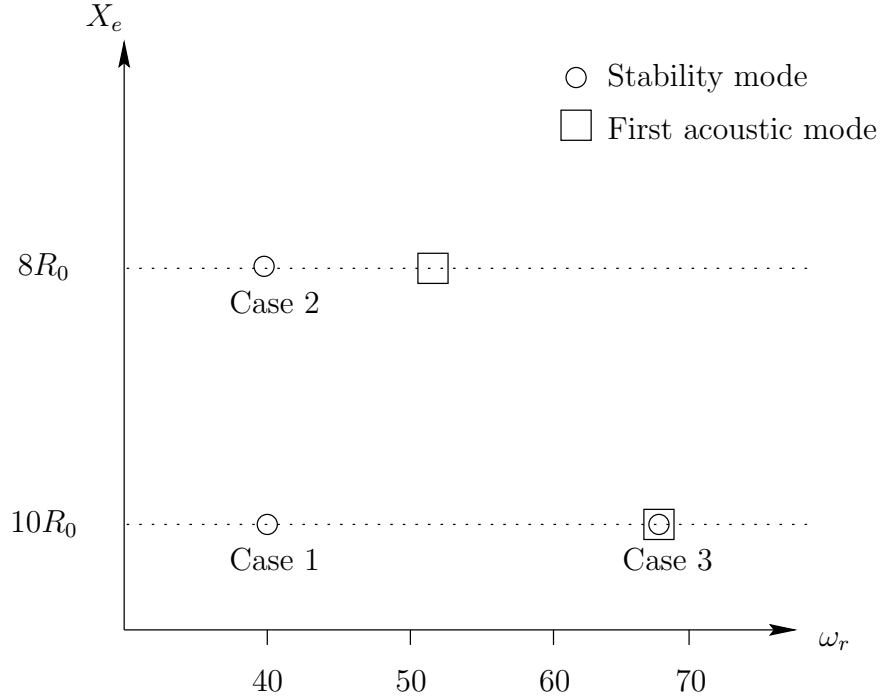


Figure 4. Sketch representing the three computed cases.

the linear stability theory. Figs. 5(a), 5(b), 5(c), 5(d), 5(e) and 5(f) show the comparisons between the signals s_{fluc}^q and the theoretical evolutions s_{th}^q for $q = u_x$ and $q = u_r$ at three different locations (which are indicated on the top of each figure ^a). The comparisons give an excellent agreement for signals of the radial velocity components : $s_{fluc}^{u_r} = s_{th}^{u_r}$, especially on Figs. 5(a) and 5(c). For the third sensor, the signal $s_{fluc}^{u_r}$ is perturbed by noise but the general behaviour corresponds to the theoretical evolution $s_{th}^{u_r}$. In fact, the spatial perturbation $(\hat{u}_r)_r$ introduced at $t = 0$ s in the computation follows its theoretical evolution which implies $(\hat{u}_r)_i$, ω_r and ω_i . Thus the circular frequency $\omega_r = 40.409$ and the temporal growth rate $\omega_i = -9.164$ are extremely well recovered by the computation.

However some differences appear on the signals of the longitudinal velocity component : $s_{fluc}^{u_x} \neq s_{th}^{u_x}$. As $s_{fluc}^{u_r} = s_{th}^{u_r}$ there must be a part of $s_{fluc}^{u_x}$ which corresponds to $s_{th}^{u_x}$. The question is to find out what can be the difference $s_{fluc}^{u_x} - s_{th}^{u_x}$. It is "obviously" a combination of acoustic modes of the pipe. One notes $s_{ac}^q = s_{fluc}^q - s_{th}^q$.

1. The acoustic boundary layer

In the case of a pipe flow induced by wall injection an analytical solution exists, it has been found by J. Majdalani *et al.*^{15,16}. Only the basics of the approach used by the authors are reminded in this paper.

Considering the compressible Navier-Stokes equations, a perturbation q of the mean flow \bar{Q} is searched. The considered mean flow is the Taylor-Culick one, which is closed to the computed one used for the calculation except in a region closed to the front wall. Thus, the final analytical solution is not valid in this little region. The perturbation q is divided into two different parts $q = \check{q} + \tilde{q}$. \check{q} is an irrotational compressible perturbation and \tilde{q} is an incompressible rotational one. In fact, one finds that \tilde{q} stands for the classical plane wave solution which is the acoustic wave solution in a pipe without flow. Thus, \tilde{q} is the correction brought to take into account the effect of the flow \bar{Q} on the plane wave \check{q} : \tilde{q} is explicitly the acoustic boundary layer.

^aThe french word "capteur" means sensor

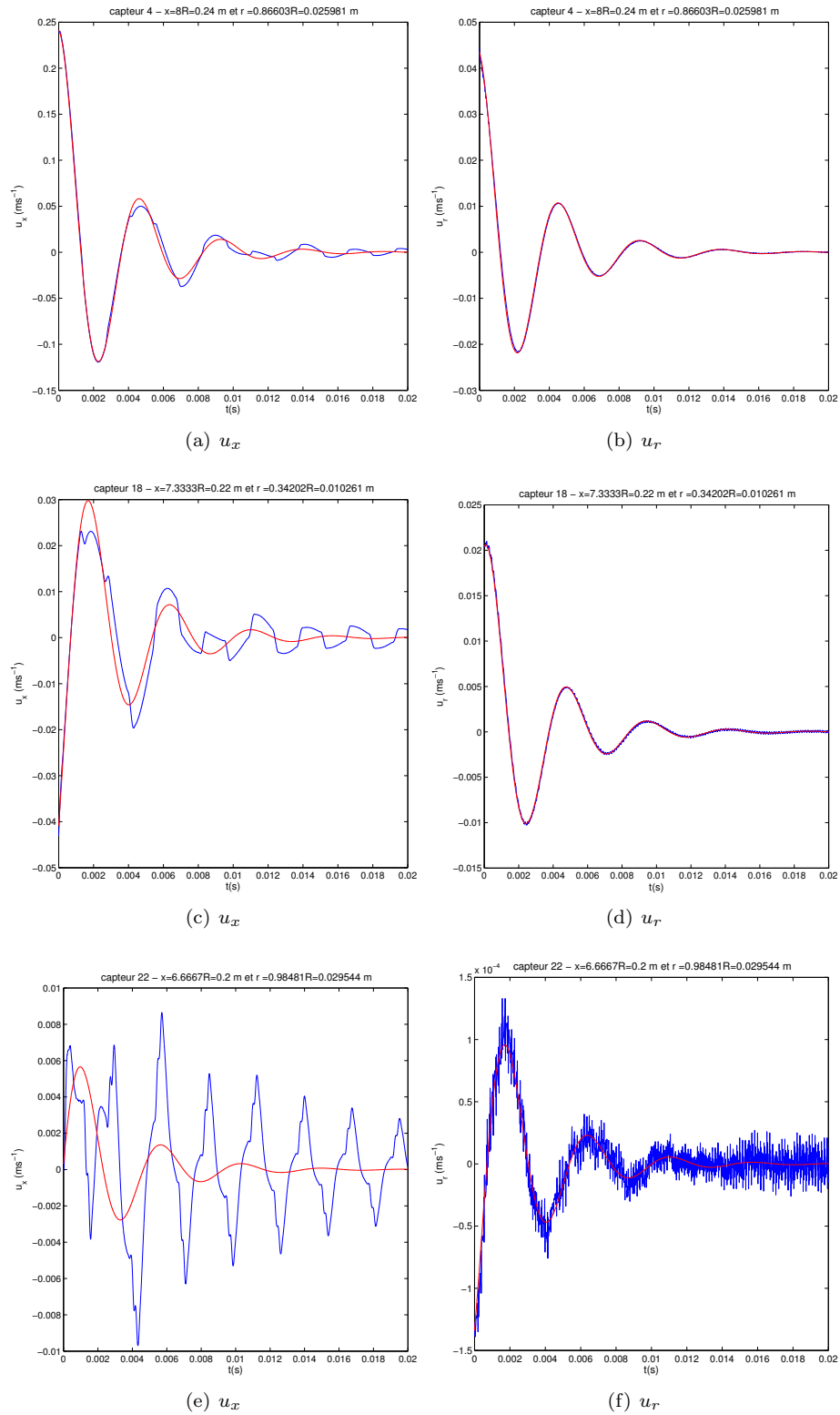


Figure 5. Case 1. Comparisons between the fluctuating part of the signal of three sensors s_{fluc}^q (blue line) and the theoretical evolutions s_{th}^q given by formula (2).

Finally one obtains :

$$\begin{cases} \check{p}(x, t) = \cos(\omega_m x) e^{-i\omega_m t} \\ \check{u}(x, t) = i \sin(\omega_m x) e^{-i\omega_m t} \underline{e}_x \end{cases} \quad (3)$$

where \check{p} and \check{u} are the pressure and velocity fluctuations of the plane wave solution. $\omega_m = (m - \frac{1}{2})\pi/L$, $m \in \mathbb{N}^*$, is the circular frequency. Concerning the acoustic boundary layer one finds :

$$\begin{cases} \tilde{u}_x = -i \sin(\theta) \sin(\omega_m x \sin(\theta)) e^{[\zeta - i(\omega_m t + \Phi)]} \\ \tilde{u}_r = -\frac{M}{r} \sin^3(\theta) \cos(\omega_m x \sin(\theta)) e^{[\zeta - i(\omega_m t + \Phi)]} \end{cases} \quad (4)$$

ζ and Φ are functions of the radial position r and are given by :

$$\begin{cases} \zeta = \zeta_0 + \zeta_1 \quad , \quad \Phi = \Phi_0 + \Phi_1 \\ \zeta_0(r) = \xi \frac{\eta(r)r^3}{\sin^3(\theta)} \quad , \quad \Phi_0(r) = \frac{S_m}{\pi} \ln \tan\left(\frac{\theta}{2}\right) \\ \zeta_1(r) = -\frac{2\pi^2}{S_m^2} \xi \frac{\eta(r)r^3}{\sin^3(\theta)} \left(\cos(2\theta) + \frac{\sin(2\theta)}{2\theta} \right) \quad , \quad \Phi_1(r) = -\frac{2\pi}{S_m} \xi \frac{\eta(r)r}{\sin^2(\theta)} \left(1 + \frac{3\theta}{\tan(\theta)} \right) \\ \xi = \frac{\omega_m^2}{M^3 Re} \quad , \quad \theta = \pi \frac{r^2}{2} \quad , \quad \eta(r) = -\frac{1-r}{1 + \frac{3}{2}(1-r)^{3/2} \left(\frac{1-r}{r} - \frac{3}{2} \ln(r) \right)} \end{cases} \quad (5)$$

Thanks to the expressions 3, 4 and 5, a complete analytical solution of acoustic modes in a pipe is available, taking into account the effect of the mean flow \bar{Q} . As mentioned before, this solution is not valid in the front wall region since the basic flow is different from the Taylor-Culick one. However, it does not have major consequences for comparisons with the DNS calculations.

The signals s_{ac}^q can be decomposed on the basis of these analytical acoustic modes to analyze them. Implicitly, we assume that the acoustics exhibited by the DNS calculation is a linear combination of acoustic modes. The coefficients of the decomposition are noted A_m .

2. Decomposition of the acoustics using a Least Square technique

Any signal s_{fluc}^p is mainly composed by the acoustics of the pipe because the stability mode pressure fluctuation is very weak, all the more so since x is small. Thus, we have $s_{fluc}^p \approx s_{ac}^p$. Given that the acoustic boundary layer for the pressure is zero, *i.e.* $\check{p} = 0$, it is more accurate to look for the coefficient A_m of the decomposition of the recorded acoustic signal on the basis of the M first analytical acoustic modes on the pressure signal s_{ac}^p . However, it could be done on $s_{ac}^{u_x}$ where the acoustic boundary layer part is non-zero. Finally, using a least square technique, the coefficient A_m of the 100 first acoustic modes are searched on the signal s_{ac}^p of a given single sensor (sensor 21 located at $x = 0.2$ m and $r = 0.03$ m). The comparison between s_{ac}^p for sensor 22 and the combination of acoustic modes is given on Fig. 6(a). On Fig. 6(b) the coefficients A_m of the combination are plotted with respect to the mode number m . To mimic the viscous dissipation which leads to the damping of the acoustics, a hand-made function F_μ is added to the combination. This function will be used for all the sensors signals whatever the physical quantity q is concerned. F_μ is only valid after the growing phase of the acoustics. In fact, at $t = 0$ s the introduction of the stability mode $\omega = 40.409 - 9.164i$ leads to a fast growing and to a slow damping (due to dissipation) of an acoustic distribution. Fig. 6(a) shows the expected good agreement. In fact, sensor 21 and 22 have the same x location and there is no radial dependance on the acoustic pressure fluctuation. One can note that the combination of acoustic modes is almost harmonic, which confirms the linear behaviour of the perturbations in this DNS calculation.

Now, the A_m coefficients of the combination are used to calculate the acoustic velocity fluctuations. Comparisons between $s_{ac}^{u_x}$ and the linear combination of acoustic modes are shown on Figs. 7(a), 7(b) and, 7(c). Once again, because of the viscous dissipation, the function F_μ is used to describe the envelop of the signals (the initial amplitude is adjusted to match the numerical results for $s_{ac}^{u_x}$. One can see that the coefficients

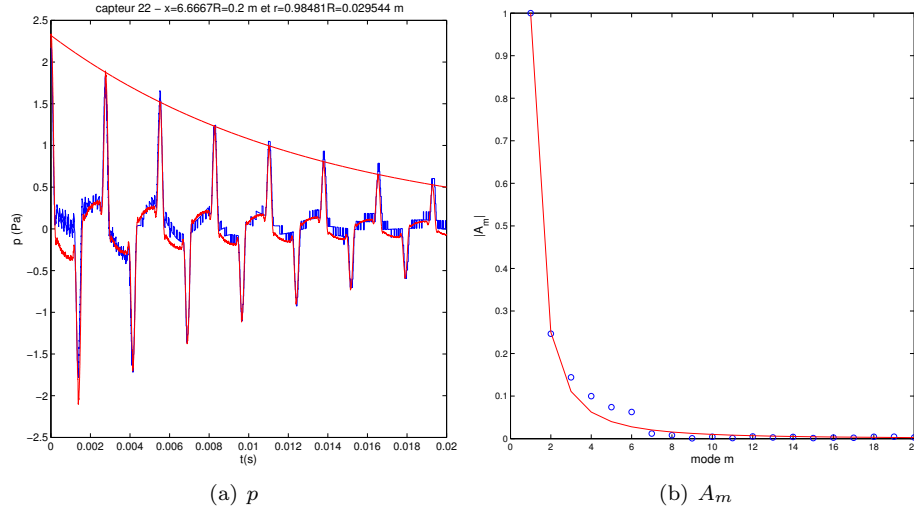


Figure 6. Case 1. Fig. 6(a) presents the comparison between the signal s_{ac}^p (blue line) and the combination of the 100 first acoustic modes (red line) for sensor 22 ($x = 0.2$ m and $r = 0.295$ m). The function F_μ is reported in red and stands for the envelope of the combination. The line Fig. 6(b) shows the values A_m of the coefficients with respect to the mode number m . they are compared to the line $\frac{1}{m^2}$.

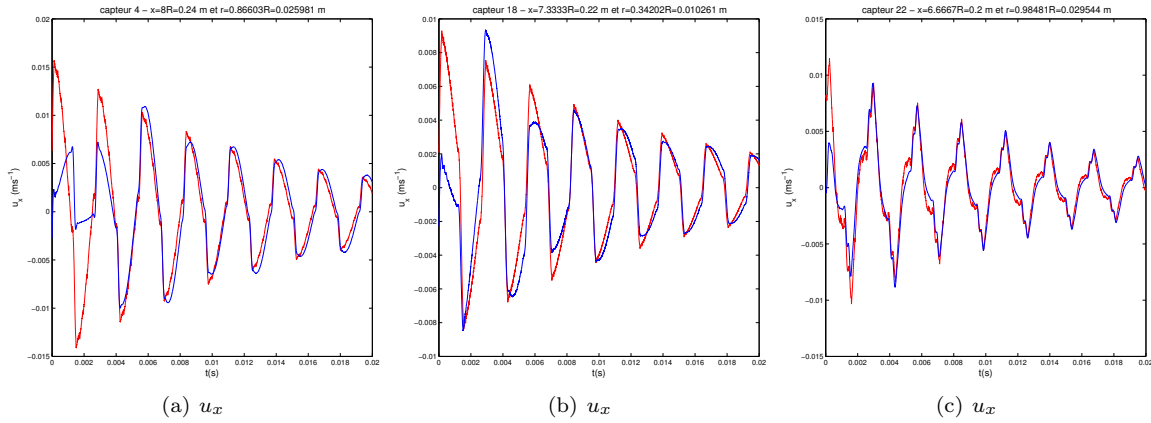


Figure 7. Case 1. Comparisons between the signals $s_{ac}^{u_x}$ of three sensors and the combination of the 100 first acoustic modes given by the coefficients A_m . The envelope of the theoretical acoustic signals is related to the function F_μ .

A_m allow to build the combination of acoustic modes which is exhibited by the DNS calculation. This proves the relevance of the approximation of the acoustic modes in a pipe for such a flow found by Majdalani *et al.*.

As a conclusion for this case where $X_e = 8R_0$ and $\omega = 40.409 - 9.164i$ it appears that the adopted strategy consisting in introducing a stability mode allows to confirms the values ω_r and ω_i found out by the linear stability analysis. However, even if it works for a particular mode, it has to be proved that when the length X_e is changed the values are changed, especially ω_i . Moreover the introduction of the mode $\omega = 40.409 - 9.164i$ has lead to to the development of a harmonic distribution os acoustic modes. These modes are well predicted by the analytical solution of Majdalani *et al.*.

B. Case 2

Here the considered mode is $\omega = 40.367 - 7.302i$ for a pipe length $X_e = 10R_0$. This mode is the mode $\omega = 40.409 - 9.164i$ which has moved to $\omega = 40.367 - 7.302i$ when X_e has changed from $X_e = 8R_0$ to $X_e = 10R_0$, see Fig. 1. As in the previous case, only the real part $(\hat{u}_x)_r$ and $(\hat{u}_r)_r$ of the mode $\omega = 40.367 - 7.302i$ are introduced at $t = 0$ s. Of course, this leads to the excitation of the acoustics. The least square method is used in this case too to calculate the combination of acoustic modes from a pressure signal. The function F_μ is still used with a new initial amplitude value to described the viscous dissipation.

Figs. 8(a), 8(b), 8(c) and 8(d) show the whole set of comparisons between signals and theoretical evolutions for sensor 94. The excellent agreement observed on all these figures indicate that the analysis we have done

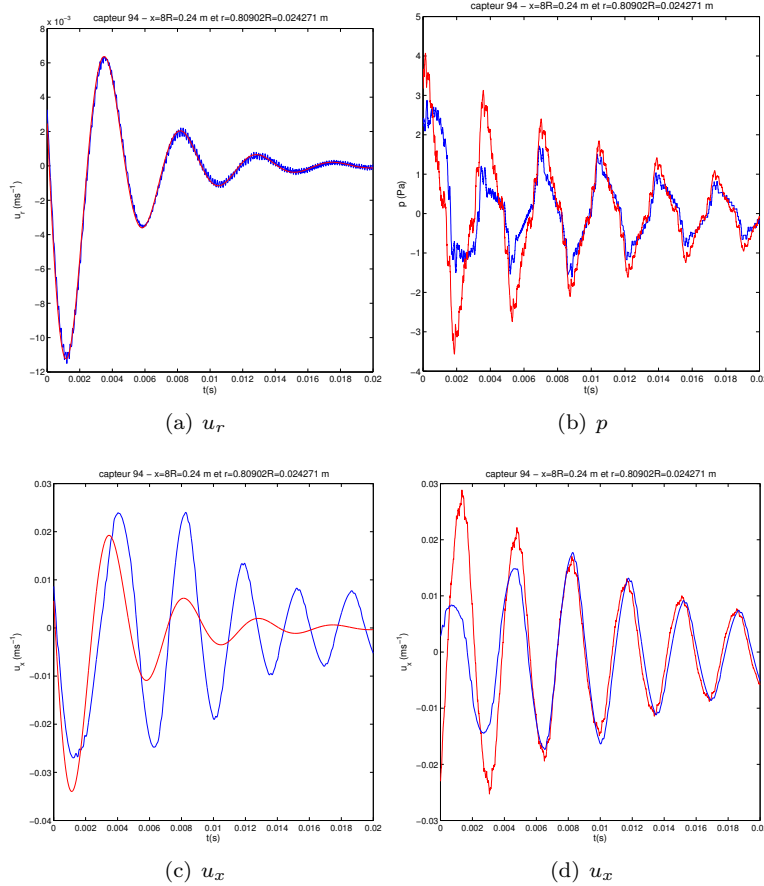


Figure 8. Case 2. The signals are all coming from sensor 94 located at $(x, r) = (8R_0, 0, 809R_0) = (0, 24 \text{ m}, 0, 0243 \text{ m})$. Figs 8(a) and 8(c) present comparisons between signals $s_{fluc}^{u_x}$ and $s_{fluc}^{u_r}$ and their respective theoretical evolutions $s_{th}^{u_x}$ and $s_{th}^{u_r}$. Figs 8(b) and 8(d) show comparisons between signals s_{ac}^p and $s_{ac}^{u_x}$ and a combination of 100 acoustic modes calculated from a pression signal picked in the section $x = R_0 = 0, 03 \text{ m}$.

is relevant. In particular, Fig. 8(a) shows that the values ω_r and ω_i given by the stability analysis are recovered by the DNS calculation. Thus, the evolution of the temporal growth rate ω_i with respect to X_e is not caused by the numerical procedure used to compute the eigenvalues of the stability problem. However, this evolution can be related to the truncature in the sense that cutting the domain in X_e means neglecting the flow outside the domain for $x > X_e$. Until now, there is no physical explanation to the dependance of ω_i with respect to X_e .

C. Case 3

The mode $\omega = 40.409 - 9.164i$ calculated for $X_e = 8R_0$ which moves to $\omega = 40.367 - 7.302i$ for $X_e = 10R_0$, has a frequency $f = 214$ Hz. This frequency is far from the first acoustic mode one $f_{ac} = \frac{c}{2\pi R_0} k_1 = \frac{c}{4X_e}$. One finds $f_{ac} = 363$ Hz for $X_e = 8R_0$ and $f_{ac} = 291$ Hz for $X_e = 10R_0$. To force the expected coupling between the acoustics and the intrinsic instabilities, it is interesting to consider a stability mode which frequency is close to an acoustic mode one.

Let consider the mode $\omega = 68.679 - 7.594i$ calculated for $X_e = 8R_0$. Its frequency, $f = 364$ Hz, is almost equal to the first acoustic mode one $f_{ac} = 363$ Hz. At $t = 0$ s this mode is introduced in the flow and the DNS calculation is started. Fig. 9(a) shows that the signal $s_{fluc}^{u_r}$ does not match the theoretical evolution given by (2). In fact, Fig. 9(b) where the FFT ^b of signal $s_{fluc}^{u_r}$ is plotted, shows that the main amplified

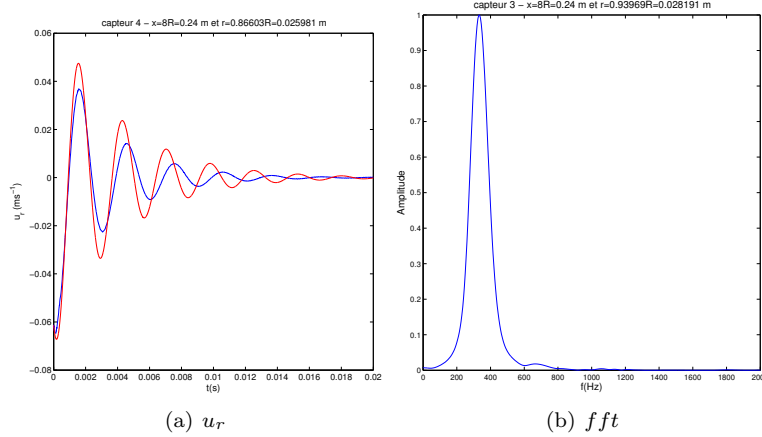


Figure 9. Case 3. **Fig. 9(a)** gives the comparison between the signal $s_{fluc}^{u_r}$ and the theoretical evolution for sensor 4. **Fig. 9(b)** shows the result of the FFT for this signal $s_{fluc}^{u_r}$.

frequency is about $f = 335$ Hz. This suggests that the stability mode $\omega = 62.787 - 7.389i$, which frequency is $f = 333$ Hz, interferes in the computation. It seems weird to note that the mode $\omega = 62.787 - 7.389i$ may be excited since its frequency is farther to the first acoustic mode one than the frequency of the introduced mode $\omega = 68.679 - 7.594i$.

In order to find the modal combination of stability modes which composes the signals $s_{fluc}^{u_r}$, a spatial decomposition is performed at each time. The signal of each sensor is believed to be made of a combination of the two stability modes $\omega = 68.679 - 7.594i$ and $\omega = 62.787 - 7.389i$ respectively determined by the complex amplitude coefficients A^{68} and A^{62} :

$$s_{fluc}^{u_r} = A_r^{62} (\hat{u}_r^{62})_r + A_i^{62} (\hat{u}_r^{62})_i + A_r^{68} (\hat{u}_r^{68})_r + A_i^{68} (\hat{u}_r^{68})_i \quad (6)$$

Using the least square method, the coefficients A^{62} and A^{68} are calculated at each time from the whole set of the sensor signals $s_{fluc}^{u_r}$. Finally, one gets two amplitude coefficients A^{62} and A^{68} depending on the time t .

Once these coefficients are known, we have to see if the combination of the two stability modes matches the signal $s_{fluc}^{u_x}$. To do so, the acoustic parts of signals $s_{fluc}^{u_x}$ must be extracted. Once again the combination of acoustic modes is calculated from a signal s_{fluc}^p , assumed to be only composed by the acoustics. Thanks to the coefficients A_m of the 100 first acoustic modes and the function F_μ , the signals $s_{ac}^{u_x}$ are theoretically known.

Using the modal decomposition A^{62} and A^{68} , one can have access to the part of the signals due to the stability modes, noted so far $s_{th}^{u_x}$. Then it is interesting to compare $s_{fluc}^{u_x} - s_{th}^{u_x}$ to the theoretical evolution of acoustic modes given by $s_{ac}^{u_x}$. Figs. 10(a), 10(b) and 10(c) give such comparisons for three distinct sensors. The good agreements prove that the modal decomposition corresponds to the intrinsic instabilities part of

^b FFT of such signals are difficult to perform because the sampling frequency is very high compared to the amplified frequencies. In practice a periodogram method is used to get the frequency signature of these signals.

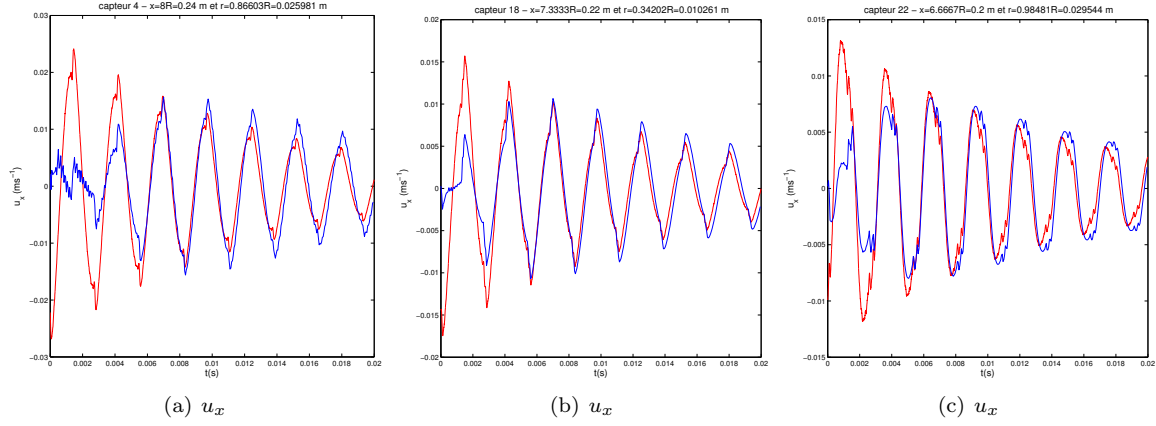


Figure 10. Case 3. Comparison between the signals $s_{fluc}^{u_x} - s_{th}^{u_x}$ and the theoretical acoustic evolution $s_{ac}^{u_x}$ for three sensors.

the signal $s_{fluc}^{u_x}$.

To go further in the analysis, it is interesting to plot the amplitude functions $|A_{62}|$ and $|A_{68}|$ and the respective phase functions $\psi^{62} = \arctan\left(\frac{A_r^{62}}{A_i^{62}}\right) = \arg(A^{62}) [2\pi]$ and $\psi^{68} = \arctan\left(\frac{A_r^{68}}{A_i^{68}}\right) = \arg(A^{68}) [2\pi]$. If the DNS calculation had exhibited purely modal evolution the amplitude functions $|A_{62}|$ and $|A_{68}|$ would have match the theoretical evolutions given by $e^{\nu^{62}t}$ and $e^{\nu^{68}t}$. Similarly, the phase functions ψ^{62} and ψ^{68} would have follow the theoretical evolutions $2\pi f^{62}t [2\pi]$ and $2\pi f^{68}t [2\pi]$. On Figs. 11(a), 11(b) and 11(c) the comparisons of $|A_{62}|$, $|A_{68}|$, ψ^{62} and ψ^{68} with their respective modal evolutions are shown. Through all

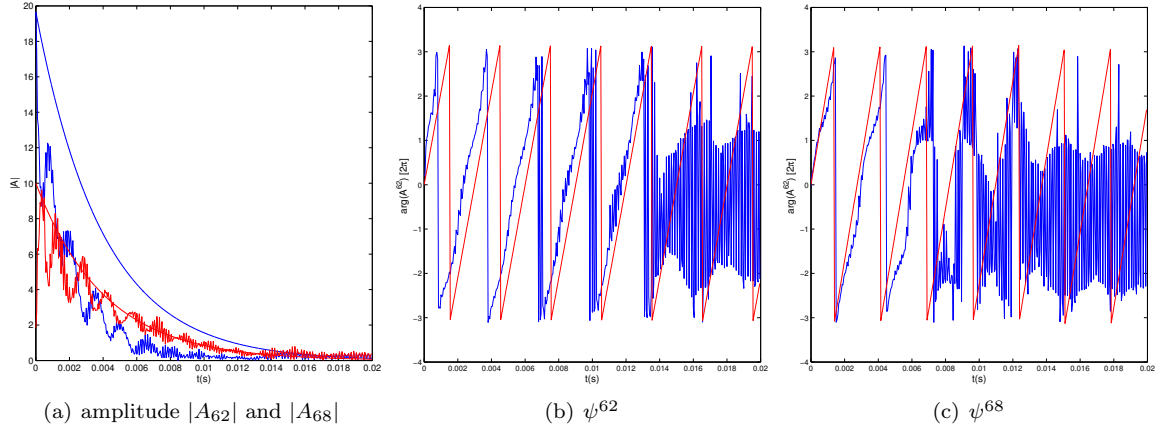


Figure 11. Case 3. Fig. 11(a) show the evolution of the amplitude of the two modes $\omega = 62.787 - 7.389i$ (red lines) and $\omega = 68.679 - 7.594i$ (blue lines). These amplitudes are compared to $10e^{\nu^{62}t}$ and $0,01A_0 \|\hat{u}_r^{68}\|_\infty e^{\nu^{68}t}$. Figs. 11(b) and 11(c) give the phase functions ψ^{62} and ψ^{68} (blue lines) compared to the theoretical evolution $2\pi f^{62}t [2\pi]$ and $2\pi f^{68}t [2\pi]$ (red lines).

these figures one can see that the introduction of mode $\omega = 68.679 - 7.594i$ has led to the development of mode $\omega = 62.787 - 7.389i$. Rapidly, the mode $\omega = 62.787 - 7.389i$ becomes dominating in the computation and it looks like it oscillates around a modal evolution. Contrary to what was expected, *i.e.* a direct interaction between the stability mode $\omega = 68.679 - 7.594i$ and the first acoustic mode, this DNS calculation exhibits a coupling mechanism between two stability modes. This is all the more strange since the mode $\omega = 62.787 - 7.389i$ is farther to the acoustic mode than the mode $\omega = 68.679 - 7.594i$. It is quite hard to explain the reasons which have led to this observation.

The very important fact illustrated by this case, is that a stability mode could merge into the flow without

being artificially introduced in it. The previous analysis has shown that the mode $\omega = 62.787 - 7.389i$ has naturally merge into the flow because of the proximity of the frequencies of mode $\omega = 68.679 - 7.594i$ and of the first acoustic mode.

V. Conclusion

In this paper the use of DNS calculations has given a new insight on the linear stability analysis results. In fact, it has been proved that the eigenvalues given by the stability results are recovered when computing the unsteady motion of an isolated mode. A special attention has been paid on the dependance of ω_i with respect to X_e . The temporal growth rate rules the stable or unstable behaviour of these modes. As ω_i is getting closer to 0 when X_e is growing, one can imagine that for a sufficiently large value of X_e , ω_i will become positive. This would mean that the mode will be unstable. But it only happens for $X_e/R > 16$ and it has been proved in cold gaz experiments that the flow is turbulent for $X_e/R > 13$. Since the flow is turbulent the linear stability analysis is not valid any more. Non linear effect are believed to act before the modes became unstable. In fact, many comparisons with cold gaz¹ and hot gaz² experiments have proved the relevance of the stability analysis which exhibit temporally stable modes. The stable nature of the intrinsic instabilities has led to a coherent scenario for the thrust oscillations arising.

In addition to the confirmation of the stability results, these DNS calculations have emphasized the quality of the analytical solution for the acoustics of the Taylor-Culick flow found by Majdalani *et al.*. Moreover, it has been shown that the proximity of the frequencies of a stability mode and of acoustic modes could lead to the merging of other stability modes. Other DNS computations made with unsteady injection velocity have highlighted the existence of a coupling between the acoustics and stability modes. For unsteady injection velocity cases, the frequency of one mode $f = \frac{V_{inj}}{2\pi R}\omega_r$ becomes a function of the time t and can cross the one of an acoustic mode f_{ac} . Thus we reproduce what happens in live motors where the coupling mechanism between acoustics and intrinsic instabilities is believed to be responsible of the merging of the frequency paths.¹

Acknowledgments

This study has been supported by the French Space Agency CNES and by ONERA. The authors thank M. Prevost and G. Avalon from ONERA for their accurate measurements, their help and their relevant advices. A special thank goes to J. Majdalani for its work on the acoustics of the Taylor-Culick flow. Our collobaration has been fruitful.

References

- ¹Chedevergne, F., Casalis, G., and Feraille, T., "Biglobal linear stability analysis of the flow induced by wall injection," *Physics of Fluids*, Vol. 18, January 2006.
- ²Chedevergne, F. and Casalis, G., "Detailed Analysis of the Thrust Oscillations in Reduced Scale Solid Rocket Motors," 42nd AIAA/ASME/SAE/ASEE Joint Propulsion Conference and Exhibit, Sacramento, California, 10-13 July 2006.
- ³Prevost, M. and Godon, J.-C., "Thrust Oscillations in Reduced Scale Solid Rocket Motors, part I : Experimental Investigations," 41st AIAA/ASME/SAE/ASEE Joint Propulsion Conference and Exhibit, Tucson, Arizona, 10-13 July 2005.
- ⁴Avalon, G. and Lambert, D., "Campagne d'essais VALDO, periode 2000/2001," Tech. Rep. RT 2/05424 DEFA, ONERA, Etablissement de Palaiseau, octobre 2001.
- ⁵Taylor, G. I., "Fluid flow in regions bounded by porous surfaces," *Proc. of the Royal Soc. Series A, London*, Vol. 234, No. 1199, 1956, pp. 456–475.
- ⁶Culick, F., "Rotational axisymmetric mean flow and damping of acoustic waves in a solid propellant rocket," *AIAA Journal*, Vol. 4, No. 8, 1966, pp. 1462–1464.
- ⁷Theofilis, V., "Advances in global linear instability analysis of nonparallel and three-dimensional flows," *Progress in Aerospace Sciences*, Vol. 39, 2003, pp. 249–315.
- ⁸Casalis, G., Chedevergne, F., Fraille, T., and Avalon, G., "Global Stability of the Flow induced by wall injection," *IUTAM, Symposium on Laminar-Turbulent Transition*, Bangalore, Inde, Dcembre, 13-17 2004.
- ⁹Golub, G. and Loan, C. V., *Matrix Computations (third edition)*, The Johns Hopkins University Press, 1996.
- ¹⁰Chevalier, P., Courbet, B., Dutoya, D., Klotz, P., Ruiz, E., Troyes, J., and Villedieu, P., "CEDRE : development and validation of a multiphysic computational software," *1st European Conference for Aerospace Sciences (EUCASS)*, Moscow, Russia, 2005.
- ¹¹Vuillot, F., Scherrer, D., and Habiballah, M., "CFD code validation for space propulsion applications," *5th International Symposium on Liquid Space Propulsion*, Chattanooga, Tennessee, E.-U., 2003.

¹²Chedevergne, F. and Casalis, G., “Front Wall boundary layer influence on the stability of the flow induced by wall injection,” 7th *ONERA DLR Aerospace Symposium*, Toulouse, France, 4-6 October 2006.

¹³Apte, S. and Yang, V., “Unsteady Flow Evolution in Porous Chamber with Surface Mass Injection, Part 1 : Free Oscillation,” *AIAA Journal*, August 2001.

¹⁴Apte, S. and Yang, V., “Unsteady Flow Evolution in Porous Chamber with Surface Mass Injection, Part 1 : Acoustic Excitation,” *AIAA Journal*, August 2001.

¹⁵Majdalani, J. and Moorhem, W. V., “Improved Time-Dependent flowfield solution for solid rocket motors,” *AIAA Journal*, Vol. 36, No. 2, February 1998.

¹⁶Majdalani, J. and Flandro, G., “The oscillatory pipe flow with arbitrary wall injection,” *Proceedings of the Royal Society, Series A*, Vol. 458, May 2002, pp. 1621–1651.